Title: The close relations between podocyte injuries and membranous proliferative glomerulonephritis in autoimmune murine models

Authors: Junpei Kimura[1], Osamu Ichii[1], Saori Otsuka[1], Hayato Sasaki[2], Yoshiharu Hashimoto[3], and Yasuhiro Kon[1]

Affiliations:

[1]Laboratory of Anatomy, Department of Biomedical Sciences, Graduate School of Veterinary Medicine, Hokkaido University, Sapporo, Japan

[2]Laboratory of Laboratory Animal Science and Medicine, Department of Disease Control, Graduate School of Veterinary Medicine, Hokkaido University, Sapporo, Japan

[3]Office for Faculty Development and Teaching Enriched Veterinary Medicine, Graduate School of Veterinary Medicine, Hokkaido University, Sapporo, Japan

Corresponding Author

Dr. Y. Kon, D.V.M., Ph.D., Laboratory of Anatomy, Department of Biomedical Sciences, Graduate School of Veterinary Medicine, Hokkaido University, Kita18-Nishi 9, Kita-ku, Sapporo, Hokkaido 060-0818, Japan. Tel.: +81-11-706-5189, Fax: +81-11-706-5189, E-mail: y-kon@vetmed.hokudai.ac.jp

Running head: Podocyte injuries in murine glomerulonephritis

Conflict of Interest Statement

The authors declare that there is no conflict of interest.

Keywords: Autoimmune disease, B6.MRL-(*D1Mit202-D1Mit403*), BXSB/MpJ, Membranous proliferative glomerulonephritis, Podocyte, Systemic lupus erythematosus

Word count: 5000 words

Abstract

[BACKGROUND] Membranous proliferative glomerulonephritis (MPGN) is a major primary cause of chronic kidney disease (CKD). Podocyte injury is crucial in the pathogenesis of glomerular disease with proteinuria, leading to CKD. To assess podocyte injuries in MPGN, the pathological features of spontaneous murine models were analyzed.

[METHODS] The autoimmune-prone mice strains BXSB/MpJ-*Yaa* and B6.MRL-(*D1Mit202-D1Mit403*) were used as the MPGN models, and BXSB/MpJ-*Yaa*$^{+}$ and C57BL/6 were used as the respective controls. In addition to clinical parameters and glomerular histopathology, the protein and mRNA levels of podocyte functional markers were evaluated as indices for podocyte injuries. The relation between MPGN pathology and podocyte injuries were analyzed by statistical correlation.

[RESULTS] Both models developed MPGN with albuminuria and elevated serum anti-dsDNA antibody levels. BXSB/MpJ-*Yaa* and B6.MRL showed severe proliferative lesions with T- and B-cell infiltrations and membranous lesions with T-cell infiltrations, respectively. Foot process effacement and microvillus-like structure formation were observed ultrastructurally in the podocytes of both MPGN models. Furthermore, both MPGN models showed a

decrease in immune-positive areas of nephrin, podocin, and synaptopodin in the glomerulus, and in the mRNA expression of *Nphs1*, *Nphs2*, *Synpo*, *Actn4*, *Cd2ap*, and *Podxl* in the isolated glomerulus. Significant negative correlations were detected between serum anti-dsDNA antibody levels and glomerular *Nphs1* expression, and between urinary albumin-to-creatinine ratio and glomerular expression of *Nphs1*, *Synpo*, *Actn4*, *Cd2ap*, or *Podxl.* [CONCLUSION] MPGN models clearly developed podocyte injuries characterized by the decreased expression of podocyte functional markers with altered morphology. These data emphasized the importance of regulation of podocyte injuries in MPGN.

Introduction

Chronic kidney disease (CKD) is one of the most serious public health problems because it is strongly associated with not only end-stage renal disease (ESRD) but also cardiovascular diseases [1]. Thus, understanding the pathophysiology of CKD is important to improve the morbidity and mortality of patients. Recent studies have shown that progressive podocyte injury, also called podocytopathy, is one of the key events in the pathogenesis of major CKD primary diseases such as diabetic nephropathy and renal sclerosis [2,3].

Podocytes are highly differentiated epithelial cells lining the outside of glomerular capillaries, and their foot processes (FPs) regulate the glomerular filtration barrier (blood–urine barrier; BUB) by the formation of a slit diaphragm (SD). Yi *et al* [4] indicated that a decrease in the expression of SD molecules and effacement of FPs were associated with the development of renal sclerosis. According to Pagtalunan *et al* [5], the number of podocytes in the glomerulus could be used as indices of podocyte injury in patients with diabetic nephropathy. In a CKD animal study targeting dogs, we have also clarified that the immune-positive levels of glomerular SD molecules, especially nephrin and actinin alpha 4 (ACTN4), negatively correlated with

serum creatinine levels, and nephrin mRNA expression in the kidneys of CKD groups was significantly lower than that in normal animals and negatively correlated with serum creatinine [6]. Several studies have indicated that the signaling pathway through Notch, transforming growth factor beta (TGF-β), and angiotensin II play crucial roles in podocyte injuries [7–10].

Membranous proliferative glomerulonephritis (MPGN) is one of the major CKD primary diseases and is associated with infections, drugs, and systemic disorders [11]. From early stage MPGN, increased glomerular cells and immune-complex depositions were observed in glomerular lesions with proteinuria caused by the ultrafiltration of plasma proteins [12]. Chronic glomerular lesions with increased urinary protein could trigger the formation of tubulointerstitial lesions and eventually progress to interstitial fibrosis leading to ESRD [12]. Although the appearance of proteinuria indicates BUB disruption in MPGN from the early stage, little is known about podocyte injury in MPGN patients and in model mice.

Spontaneous MPGN models, lupus-prone mice such as NZB, (NZB × NZW) F1 hybrid, BXSB/MpJ-*Yaa* (BXSB-*Yaa*), and MRL/MpJ-*lpr* are commonly used. These strains develop systemic autoimmune diseases

characterized by increased serum autoantibody levels and vasculitis, as well as MPGN [13–15]. BXSB-*Yaa* carries a mutant gene located on the Y chromosome, designated as Y-linked autoimmune acceleration (*Yaa*), and males show more severe MPGN than females [16]. We have demonstrated that BXSB-*Yaa* mice develop glomerular lesions with decreased WT1-positive podocytes leading to proteinuria subsequent to tubulointerstitial lesion formation [17]. Furthermore, we developed a spontaneous CKD model named B6.MRL- (*D1Mit202-D1Mit403*) (B6.MRL), carrying the C57BL/6 (B6) background and the telomeric regions of chromosome 1 (68–81 cM) derived from lupus-prone MRL/MpJ [18]. This congenic region contains the Fas ligand, interferon activated gene 200 family, and Fc gamma receptor family, which were strongly associated with the developments of autoimmunity and MPGN [18]. With age, female B6.MRL spontaneously develop MPGN similar to human CKD [18-20]. Therefore, we considered that BXSB-*Yaa* and B6.MRL as appropriate models for the investigation of podocyte injury in MPGN.

In this study, the pathological features of MPGN were analyzed using 2 murine models, BXSB-*Yaa* and B6.MRL, with focus on podocyte injuries. The results showed that these MPGN models clearly developed podocyte injuries,

characterized by the decreased mRNA and protein levels of its functional markers with morphological changes and exacerbation of clinical parameters. Our data emphasized the importance of regulation of podocyte injuries in MPGN.

Materials and Methods

Animals and Sample Preparations

Experimental animals were handled according to the "Guide for the Care and Use of Laboratory Animals" of Hokkaido University, Graduate School of Veterinary Medicine (approved by the Association for Assessment and Accreditation of Laboratory Animal Care International). Male BXSB-*Yaa* and female B6.MRL were used as MPGN model mice at age 4 months and 9–15 months, respectively. As healthy controls, male BXSB/MpJ-*Yaa*$^{+}$ (BXSB) and female B6 mice were used at age 4 and 9 months, respectively. B6.MRL was created in our laboratory [18], whereas B6, BXSB, and BXSB-*Yaa* were purchased from Japan SLC Inc. (Shizuoka, Japan). All mice were maintained under specific pathogen-free conditions. The animals were subjected to deep anesthesia (60 mg/kg pentobarbital sodium administered intraperitoneally), and urine was collected by bladder puncture. After urine collection, the mice were euthanized by exsanguination from the carotid artery, and serum and kidneys were collected. The kidneys were fixed by 4% paraformaldehyde (PFA) in 0.1 M phosphate buffer (PB; pH 7.4) or 2.5% glutaraldehyde in 0.1 M PB at 4°C for histopathological analysis. PFA-fixed paraffin sections (2 μm thick) were then prepared and used for

periodic acid Schiff (PAS) staining or immunostaining.

Histological Analysis

To assess the severity of glomerulonephritis, semiquantitative glomerular damage scoring was performed as previous study [17]. Details of the procedures were described in Supplementary material 1.

Glomerular Isolation

Glomeruli of mice were isolated by a bead perfusion method [21]. Briefly, 40 mL of Hanks' balanced salt solution (HBSS) containing 8×10^7 Dynabeads (Life Technologies, Palo Alto, CA) was perfused from the left ventricle. The kidneys were removed and digested in collagenase (1 mg/mL collagenase A [Roche, Basel, Switzerland] and 100 U/mL deoxyribonuclease I [Life Technologies] in HBSS) at 37°C for 30 min. The digested tissue was gently pressed through a 100-μm cell strainer (BD Falcon, Franklin Lakes, NJ, USA) using a flattened pestle, and the cell suspension was centrifuged at $200 \times g$ for 5 min. The cell pellet was resuspended in 2 mL HBSS. Finally, glomeruli containing Dynabeads were gathered by a magnetic particle concentrator (Life Technologies).

Serological and Urinary Analysis

For the evaluation of the systemic autoimmune condition, serum levels of anti-double strand DNA (dsDNA) antibody were measured using Mouse Anti-dsDNA Ig's (Total A+G+M) ELISA kit (Alpha Diagnostic International, San Antonio, TX, USA). For the evaluation of renal function, serum blood urea nitrogen (sBUN) and creatinine (sCre) levels in all animals were measured using Fuji Drichem 7000v (Fujifilm, Tokyo, Japan). Urinary albumin-to-creatinine ratio (uACR) was determined using Albuwell M and The Creatinine Comparison (Exocell, Philadelphia, PA, USA).

Immunohistochemistry and Histoplanimetry

Immunostaining for nephrin, podocin, synaptopodin, CD3, and B220 was performed according to the procedure shown in Table 1. Details of the procedures are described in Supplementary material 1.

Quantifications of positive immunohistochemical reactions of SD molecules were performed as described previously [6]. Briefly, the glomerulus area and black pixels of positive reaction were measured, and the number of pixels per area was calculated for each SD molecule by means of

BZII-Analyzer (Keyence, Osaka, Japan). To evaluate T-cell and B-cell infiltration into the glomeruli, the number of CD3- and B220-positive cells was counted. In these measurements, 20 glomeruli were counted in 1 kidney section in each group (n = 5), and the values were expressed as means.

Immunofluorescence

Immunofluorescence for nephrin, podocin, and synaptopodin was performed according to the procedure shown in Table 1 and Supplementary material 1. Finally, the sections were examined under a fluorescence microscope (BZ-9000, Keyence).

Electron Microscopy

Ultrastructural analysis with a transmission electron microscope (TEM) was performed according to the following procedure. After fixation with 2.5% glutaraldehyde in 0.1 M PB for 4 h, small pieces of kidney tissue were fixed with 1% osmium tetroxide in 0.1 M PB for 2 h, dehydrated by graded alcohol, and embedded in epoxy resin (Quetol 812 Mixture; Nisshin EM, Tokyo, Japan). Ultrathin sections (70 nm) were double stained with uranyl acetate and lead citrate. All samples were observed under a JEOL transmission

electron microscope (JEM-1210; JEOL, Tokyo, Japan). Ultrastructural analysis with a scanning electron microscope (SEM) was performed according to the following procedure. Quarter sizes of glutaraldehyde-fixed kidneys were kept in 2% tannic acid for 1 h at 4°C and postfixed with 1% osmium tetroxide in 0.1 M PB for 1 h. The specimens were dehydrated through graded alcohol, transferred into 3-methylbutyl acetate, and dried using an HCP-2 critical point dryer (Hitachi, Tokyo, Japan). The dried specimens were sputter-coated with Hitachi E-1030 ion sputter coater (Hitachi), and then examined on an S-4100 SEM (Hitachi) with an accelerating voltage of 20 kV.

Reverse Transcription and Real-time Polymerase Chain Reaction

For the examination of mRNA expression, total RNA from isolated glomeruli was purified using RNeasy Mini Kit (Qiagen, Hilden, Germany). Total RNAs were synthesized to cDNAs by a reverse transcription (RT) reaction by using ReverTra Ace reverse transcriptase enzyme (Toyobo, Osaka, Japan) and random dT primers (Promega, Madison, WI). Each cDNA was used for real-time polymerase chain reaction (PCR) with Brilliant III SYBR Green QPCR master mix on Mx3000P (Agilent Technologies, La Jolla, CA,

USA). The expression levels of genes were normalized to actin beta (*Actb*) as a housekeeping gene. The appropriate primer pairs are shown in Table 2.

Statistical Analysis

Results were expressed as the mean ± standard error (S.E.) and statistically analyzed using a nonparametric Mann–Whitney *U* test ($P < 0.05$). The correlation between 2 parameters was analyzed using Spearman's rank correlation test ($P < 0.05$).

Results

Clinical Parameters of Membranous Proliferative Glomerulonephritis Models

As the index of the systemic autoimmune condition, the serum anti-dsDNA level of BXSB-*Yaa* and B6.MRL was significantly higher than that of BXSB and B6, respectively (Table 3). BXSB-*Yaa* showed significantly higher anti-dsDNA levels than B6.MRL. In the indices of renal functions, including sBUN, sCre, and uACR, every parameter of BXSB-*Yaa* and B6.MRL was higher than that of BXSB and B6, respectively. Significant differences between controls and MPGNmodels were observed in uACR. The uACR in BXSB-*Yaa* was significantly higher than that in B6.MRL.

Glomerular Histopathology in Membrane ProliferativeGlomerulonephritis Models

Both BXSB-*Yaa* and B6.MRL mice developed membranoproliferative MPGN characterized by glomerular hypertrophy, increased mesangial cells and their matrix, and thickening of the glomerular basement membrane (GBM) (Fig. 1b,d, Table 4). Proliferative and membranous lesions, in particular, were more severe in BXSB-*Yaa* and B6.MRL, respectively. No

glomerular lesion was observed in the controls (Fig. 1a,b, Table 4). To assess the glomerular infiltration of immune cells, immunohistochemistry for CD3 (T-cell marker) and B220 (B-cell marker) was performed. CD3-positive cells were observed in the glomerulus of BXSB-*Yaa* and B6.MRL as well as in the renal interstitium (Fig. 1f,h), but not in controls (Fig. 1e,g). Although few B220-positive cells were observed in the glomerulus of BXSB and BXSB-*Yaa* (Fig. 1i,j), they were scarcely observed in B6 and B6.MRL (Fig. 1k,l). In histoplanimetry, the number of CD3-positive cells in the glomerulus was significantly higher in both MPGN models than in each control (Fig. 1m). In relation to the histological observation, the number of B220-positive cells in the glomerulus was significantly higher in BXSB and BXSB-*Yaa* than in B6 and B6.MRL, respectively. No significant difference was observed between the controls and the MPGN models (Fig. 1m).

Glomerular Ultrastructure in Membranous ProliferativeGlomerulonephritis Models

To analyze the morphological changes of podocytes in MPGN, the glomerular ultrastructure of MPGNmodels was compared with that of the controls by TEM and SEM. Under TEM observation, the controls showed

clear cytotrabecula (Cyto, which also known as primary process) and cytopodium (FP, which is also known as secondary process) (Fig. 2a,c,f,h). In both MPGN models, FPs showed irregular arrangements with hypertrophy and partial fusions (Fig. 2b,d,e,g,i,j). Furthermore, in MPGN models, the GBM was thickened and wrinkled, and high electron-dense deposits resembling immune complexes were observed in the double-countered GBM of the subendothelial regions (Fig. 2b,d,e,g,i,j). At higher magnifications, the liner SD was clearly observed between FPs of control mice (Fig. 2f,h). In both MPGN models, FP effacement was clearly observed, but the SD and the 3-layer structure of the GBM were unclear (Fig. 2g,i,j).

Under SEM observation, the width of the cytotrabecula was increased in MPGN models compared with the controls and the FPs were unclear in the former podocytes (Fig. 2k–t). At higher magnifications, the engagements of each FP were irregular, and a microvillus-like process was observed in the surface of podocytes in both MPGN models (Fig. 2q,s,t). In B6.MRL mice podocyte, these morphological changes were observed in TEM and SEM and severer at 15 months than at 9 months.

Localization and Expression of Slit Diaphragm Molecules in Membranous

Proliferative Glomerulonephritis Models

For the evaluation of podocyte injury, immunohistochemistry and immunofluorescence for SD molecules (nephrin, podocin, and synaptopodin) were performed (Fig. 3). Linear-positive reactions for nephrin, podocin, and synaptopodin were observed along the glomerular capillary rete in controls (Fig. 3a,c,e,g,i,k). In contrast, those in the MPGN models tended to be faint, partially showed granular patterns, and localized to the glomerular edge rather than the center (Fig. 3b,d,f,h,j,l). In immunohistoplanimetry, the relative positive areas of all SD molecules in the glomerulus were significantly smaller in both MPGN models than in controls (Fig. 3m).

Furthermore, to evaluate the relation between immune cell infiltration and podocyte injuries, immune cell number (B220- and CD3-positive cells) and the relative SD molecule–positive area (nephrin, podocin, synaptopodin) in the glomerulus were analyzed (Table 5). No significant correlation was detected between both parameters.

mRNA Expression of Podocyte Functional Markers in Membranous Proliferative Glomerulonephritis Models

For further investigation of podocyte injury, the mRNA expression of the

functional markers were evaluated by quantitative PCR by using glomeruli isolated by bead perfusion methods (Fig. 4). As markers of functional proteins, *Nphs1*, *Nphs2*, and *Synpo* (SD molecules); *Actn4*, *Cd2ap*, and *Myh9* (cytoskeletal proteins); and *Podxl* (the major constituent of podocyte glycocalyx) were examined. The mRNA expression levels of all podocyte functional markers except *Myh9* were significantly decreased in BXSB-*Yaa* compared with BXSB. In the early MPGN stage of B6.MRL1 (9 months), the expression levels of *Nphs2*, *Actn4*, and *Myh9* tended to be higher than those of B6; the reverse was true for *Nphs1*, *Synpo*, and *Cd2ap*. In the late MPGN stage of B6.MRL1 (12 months), the expression levels of all functional marker mRNAs were significantly lower compared with B6.

Furthermore, the relations between clinical parameters and the mRNA expression levels of podocyte functional markers were evaluated (Table 6). Serum anti-dsDNA levels were negatively correlated with the values of *Nphs1* and *Actn4* in BXSB-*Yaa* mice, and with *Nphs1* and *Podxl* in B6.MRL. Furthermore, uACR levels were negatively correlated with the mRNA expression levels of all functional markers in both BXSB-*Yaa* and B6.MRL.

Discussion

Podocyte Injuries in Membranous Proliferative Glomerulonephritis

Systemic lupus erythematosus (SLE) is a representative autoimmune disease showing the deposition of immune complexes or direct autoantibody deposition to systemic organs, including the kidney, leading to complement activation, Fc receptor ligation, and subsequent inflammation [22]. In particular, SLE-related MPGN (lupus nephritis) is one of the most serious SLE complications since it is a major predictor of poor prognosis [22,23]. In lupus nephritis, it has been suggested that glomerular immune complex depositions cause glomerular lesions such as mesangial cell proliferation and GBM thickening, which lead to BUB disruption, as in other MPGNs such as IgA nephropathy and drug-induced glomerulonephritis [17–20,24]. BXSB-*Yaa* and B6.MRL are spontaneous murine models of autoimmune-mediated MPGN [17-20]. The present study clarified that both MPGN models had clearly elevated serum dsDNA antibody levels and developed membranoproliferative MPGN with immune complex depositions and altered podocyte morphology, such as FP effacement and the appearance of microvillus-like processes. Furthermore, the glomerular mRNA levels of podocyte functional markers were significantly decreased and negatively

correlated with uACR in the MPGN models. Little has been known about podocyte injury in MPGN, which is one of the major primary diseases leading to CKD and subsequent ESRD. The present study clarified that the decrease of podocyte functional mRNA expression levels in MPGN closely correlated with the morphological changes of podocytes as well as glomerular dysfunction indicated by increased uACR. Importantly, although the pathological mechanism of podocyte injuries was mainly investigated by using drug-induced glomerular disease models but not spontaneous models such as BXSB-*Yaa* or B6.MRL. The podocyte injuries in spontaneous models would more clearly reflect those in human clinical cases than the drug induced glomerular disease models. Recent experimental and clinical studies have revealed that podocytes exhibit various structural changes, including FP effacement, cell body attenuation, pseudocyst formation, hypertrophy, cytoplasmic accumulation of lysosomal elements, and detachment from the GBM, under several pathological situations [25]. Among these changes, FP effacement is the most representative change in podocyte shape, which is closely correlated with progressive proteinuria [26, 27]. Furthermore, an increase in podocyte microvilli represents another morphologic alteration during both experimental and human nephrotic syndrome, with unknown

mechanisms and significance [28]. These findings suggested that immune-mediated MPGNinvolves podocyte injury with morphological change leading to BUB disruption, similar to other glomerular diseases.

Contribution of Immune Cell Infiltration to Podocyte Injuries in Membranous Proliferative Glomerulonephritis

Interestingly, there was a difference in glomerular pathological features between BXSB-*Yaa* and B6.MRL; proliferative and membranous lesions were more severe in BXSB-*Yaa* and B6.MRL, respectively. Furthermore, the populations of glomerulus-infiltrating immune cells were different between these models; B-cells were localized in the glomerulus of BXSB-*Yaa,* but not B6.MRL. Because BXSB also had B-cells in the glomerulus, the BXSB genomic background rather than the *Yaa* mutation might have a role in the infiltration of B-cells in the glomerulus. Studies on lupus models have demonstrated that infiltrating B-cells in the kidney secrete antibodies with various antigen specificities, contributing to increased *in situ* immune complexes [29]. Recent reports have suggested that depleting B-cells either before or after disease onset prevented and/or delayed the onset of nephritis in several different lupus model mice [30,31]. Furthermore, lupus-prone

MRL/MpJ-*lpr* mice, which express a mutant transgene encoding surface immunoglobulin (meaning that their B-cells are unable to secrete antibodies), still develop nephritis [32]. These reports indicated that B-cells can play some roles not only in antibody productions and the activation of pathogenic T-cells but also in secreting pro-inflammatory cytokines such as tumor necrosis factor alpha (TNF-α) and interleukin 6 (IL-6), contributing to the development of glomerular lesions. However, our study demonstrated that no significant correlation was observed between T-cells or B-cells and SD protein expression levels in the glomerulus of MPGN models. From these findings, the presence and functional activation of infiltrating B-cells in the glomerulus might exacerbate the glomerular proliferative lesions in BXSB-*Yaa*, not primarily contributing to podocyte injury.

Putative Mechanism of Podocyte Injuries in Membranous Proliferative Glomerulonephritis

Recently, it has been suggested that FP effacement, the response of the podocyte to injury, is dependent on the disruption of the actin cytoskeletal network as an initial event [33,34]. In several glomerular diseases of human and mice, it has been implicated that the molecular framework of process

consists of actin filaments and cytoskeleton proteins such as ACTN4, CD2-associated protein (CD2AP), and myosin, heavy chain 9, non-muscle (MYH9), and FP effacement is caused by rearrangements of this molecular framework [33-36]. Indeed, our data indicated that the glomerular mRNA expression levels of actin-associated cytoskeletal proteins, including *Actn4* and *Cd2ap*, decreased in MPGN models compared with controls. Interestingly, the glomerular *Actn4* mRNA expression in both MPGN models strongly and negatively correlated with uACR. In contrast, the glomerular *Myh9* expression level of B6.MRL in the early stage (age 9 months) was significantly higher than that of controls. From these findings, altered glomerular mRNA expression levels of cytoskeletal proteins might indicate cytoskeletal rearrangements associated with MPGNprogression and may be associated with the effacement of FPs and formation of microvillus-like processes in podocytes.

Trigger and Crucial Pathway of Podocyte Injuries in Membranous Proliferative Glomerulonephritis

Several factors, including genetic, mechanical, and immunological stresses, and toxins, were suggested to be the causes of FP effacement

associated with cytoskeletal rearrangement and redistribution of SD proteins [37]. In the present study, MPGN podocytes showed not only morphological changes but also abnormalities in SD protein localization; nephrin, podocin, and synaptopodin were localized to the cell body as well as FP, showing a granular pattern. More recent studies indicated that Rho-kinases play a pivotal role in the organization of the actin cytoskeleton of podocytes [38-40]. Asanuma *et al* [39] suggested that Rho-kinase regulates actin–myosin-containing stress fibers in the podocyte cell body. Meyer-Schwesinger *et al* [40] demonstrated that increased activation of Rho-kinases leads to cytoskeletal rearrangement in the course of antibody-mediated podocyte injury, culminating in FP effacement, proteinuria, and detachment into the urine, and that this could be prevented by Rho-kinase inhibition. Furthermore, *in vitro* and *in vivo* studies have revealed that proinflammatory cytokines such as IL-1β and TNF-α are involved in Rho-kinase pathway activation [41,42]. From these findings, Rho-kinase abnormality, which is caused by the glomerular exposure of internal or blood proinflamatory cytokines, including IL-1β and TNF-α, might be a trigger for podocyte injury in MPGN. The determination of the immune-mediated pathological pathway of podocyte injuries would lead to

the regulation of animal and human MPGN.

In conclusion, although there was a small difference in glomerular pathological features between BXSB-*Yaa* and B6.MRL, both MPGN models clearly developed podocyte injuries characterized by decreased expression of functional markers, with morphological changes and aggravation of clinical parameters.

Acknowledgments

This work was supported by a Grants-in-Aid for Scientific Research from Graduate School of Veterinary Medicine, Hokkaido University, and Grant-in-Aid for JSPS Fellows (No. 25000961), and Grant-in-Aid for Young Scientist (No. 24688033) and Grant-in-Aid for Scientific Research B (No. 24380156) from the Ministry of Education, Culture, Sports, Science, and Technology of Japan.

References

1. Tonelli M, Wiebe N, Culleton B, House A, Rabbat C, Fok M, McAlister F, Garg AX. Chronic kidney disease and mortality risk: a systematic review. J Am Soc Nephrol 2006; 17: 2034-2047.
2. Diez-Sampedro A, Lenz O, Fornoni A. Podocytopathy in diabetes: a metabolic and endocrine disorder. Am J Kidney Dis 2011; 58: 637-646.
3. Kretzler M. Role of podocytes in focal sclerosis: defining the point of no return. J Am Soc Nephrol 2005; 16: 2830-2832.
4. Yi F, dos Santos EA, Xia M, Chen QZ, Li PL, Li N. Podocyte injury and glomerulosclerosis in hyperhomocysteinemic rats. Am J Nephrol 2007; 27: 262-268.
5. Pagtalunan ME, Miller PL, Jumping-Eagle S *et al*. Podocyte loss and progressive glomerular injury in type II diabetes. J Clin Invest 1997; 99: 342-348.
6. Ichii O, Yabuki A, Sasaki N, Otsuka S, Ohta H, Yamasaki M, Takiguchi M, Namiki Y, Hashimoto Y, Endoh D, Kon Y. Pathological correlations between podocyte injuries and renal functions in canine and feline chronic kidney diseases. Histol Histopathol 2011; 26: 1243-1255.
7. Niranjan T, Bielesz B, Gruenwald A, Ponda MP, Kopp JB, Thomas DB,

Susztak K. The Notch pathway in podocytes plays a role in the development of glomerular disease. Nat Med 2008; 14: 290-298.

8. Schiffer M, Bitzer M, Roberts IS, Kopp JB, ten Dijke P, Mundel P, Böttinger EP. Apoptosis in podocytes induced by TGF-beta and Smad7. J Clin Invest 2001; 108: 807-816.
9. Zhang C, Hu JJ, Xia M, Boini KM, Brimson C, Li PL. Redox signaling via lipid raft clustering in homocysteine-induced injury of podocytes. Biochim Biophys Acta 2009; 1803: 482-491.
10. Lavoz C, Rodrigues-Diez R, Benito-Martin A, Rayego-Mateos S, Rodrigues-Diez RR, Alique M, Ortiz A, Mezzano S, Egido J, Ruiz-Ortega M. Angiotensin II contributes to renal fibrosis independently of Notch pathway activation. PLoS One 2012; 7: e40490.
11. Kawasaki Y. Mechanism of onset and exacerbation of chronic glomerulonephritis and its treatment. Pediatr Int 2011; 53: 795-806.
12. Kriz W, LeHir M. Pathways to nephron loss starting from glomerular diseases—insights from animal models. Kidney Int 2005; 67: 404-419.
13. Li L, Nukala S, Du Y, Han J, Han J, Liu K, Hutcheson J, Pathak S, Li Q, Mohan C. Murine lupus strains differentially model unique facets of human lupus serology. Clin Exp Immunol 2012; 168: 178-185.

14. Moser K, Kalies K, Szyska M, Humrich JY, Amann K, Manz RA.. CXCR3 promotes the production of IgG1 autoantibodies but is not essential for the development of lupus nephritis in NZB/NZW mice. Arthritis Rheum 2012; 64: 1237-1246.
15. Okamoto A, Fujio K, Tsuno NH, Takahashi K, Yamamoto K. Kidney-infiltrating $CD4^+$ T-cell clones promote nephritis in lupus-prone mice. Kidney Int 2012; 82: 969-979.
16. Subramanian S, Tus K, Li QZ, Wang A, Tian XH, Zhou J, Liang C, Bartov G, McDaniel LD, Zhou XJ, Schultz RA, Wakeland EK. A Tlr7 translocation accelerates systemic autoimmunity in murine lupus. Proc Natl Acad Sci U S A 2006; 103: 9970-9975.
17. Kimura J, Ichii O, Otsuka S, Kanazawa T, Namiki Y, Hashimoto Y, Kon Y. Quantitative and qualitative urinary cellular patterns correlate with progression of murine glomerulonephritis. PLoS One 2011; 6: e16472.
18. Ichii O, Konno A, Sasaki N, Endoh D, Hashimoto Y, Kon Y. Autoimmune glomerulonephritis induced in congenic mouse strain carrying telomeric region of chromosome 1 derived from MRL/MpJ. Histol Histopathol 2008; 23: 411-422.
19. Ichii O, Konno A, Sasaki N, Endoh D, Hashimoto Y, Kon Y. Altered

balance of inhibitory and active Fc gamma receptors in murine autoimmune glomerulonephritis. Kidney Int 2008; 74: 339-347.

20. Ichii O, Otsuka S, Sasaki N, Yabuki A, Ohta H, Takiguchi M, Hashimoto Y, Endoh D, Kon Y. Local overexpression of interleukin-1 family, member 6 relates to the development of tubulointerstitial lesions. Lab Invest 2010; 90: 459-475.
21. Takemoto M, Asker N, Gerhardt H, Lundkvist A, Johansson BR, Saito Y, Betsholtz C. A new method for large scale isolation of kidney glomeruli from mice. Am J Pathol 2002; 161: 799-805.
22. Tsokos GC. Systemic lupus erythematosus. N Engl J Med 2011; 365: 2110-2121.
23. Waldman M, Appel GB. Update on the treatment of lupus nephritis. Kidney Int 2006; 70: 1403-1412.
24. Nowling TK, Gilkeson GS. Mechanisms of tissue injury in lupus nephritis. Arthritis Res Ther 2011; 13: 250.
25. Kriz W, Gretz N, Lemley KV. Progression of glomerular diseases: Is the podocyte the culprit? Kidney Int 1998; 54: 687–697.
26. Inokuchi S, Shirato I, Kobayashi N, Koide H, Tomino Y, Sakai T. Re-evaluation of foot process effacement in acute puromycin

aminonucleoside nephrosis. Kidney Int 1996; 50: 1278–1287.
27. Shirato I. Podocyte process effacement in vivo. Microsc Res Tech 2002; 57: 241-246.
28. Hara M, Yanagihara T, Hirayama Y, Ogasawara S, Kurosawa H, Sekine S, Kihara I. Podocyte membrane vesicles in urine originate from tip vesiculation of podocyte microvilli. Hum Pathol 2010; 41: 1265-1275.
29. Espeli M, Bokers S, Giannico G, Dickinson HA, Bardsley V, Fogo AB, Smith KG. Local renal autoantibody production in lupus nephritis. J Am Soc Nephrol 2011; 22: 296-305.
30. Bekar KW, Owen T, Dunn R, Ichikawa T, Wang W, Wang R, Barnard J, Brady S, Nevarez S, Goldman BI, Kehry M, Anolik JH. Prolonged effects of short-term anti-CD20 B cell depletion therapy in murine systemic lupus erythematosus. Arthritis Rheum 2010; 62: 2443-2457.
31. Ramanujam M, Bethunaickan R, Huang W, Tao H, Madaio MP, Davidson A. Selective blockade of BAFF for the prevention and treatment of systemic lupus erythematosus nephritis in NZM2410 mice. Arthritis Rheum 2010; 62: 1457-1468.
32. Chan OT, Hannum LG, Haberman AM. A novel mouse with B cells but lacking serum antibody reveals an antibodyindependent role for B cells in

murine lupus. J Exp Med 1999; 189: 1639-1648.
33. Shirato I, Sakai T, Kimura K, Tomino Y, Kriz W. Cytoskeletal changes in podocytes associated with foot process effacement in Masugi nephritis. Am J Pathol 1996; 148: 1283-1296.
34. Asanuma K, Kim K, Oh J, Giardino L, Chabanis S, Faul C, Reiser J, Mundel P. Synaptopodin regulates the actin bundling activity of alpha-actinin in an isoform-specific manner. J Clin Invest 2005; 115: 1188-1198.
35. Durvasula RV, Shankland SJ. Podocyte injury and targeting therapy: an update. Curr Opin Nephrol Hypertens 2006; 15: 1-7.
36. Asanuma K, Yanagida-Asanuma E, Takagi M, Kodama F, Tomino Y. The role of podocytes in proteinuria. Nephrology 2007; 12 Suppl 3: S15-20.
37. Asanuma K, Mundel P. The role of podocytes in glomerular pathobiology. Clin Exp Nephrol 2003; 7: 255-259.
38. Shibata S, Nagase M, Fujita T. Fluvastatin ameliorates podocyte injury in proteinuric rats via modulation of excessive Rho signaling. J Am Soc Nephrol 2006; 17: 754-764.
39. Asanuma K, Yanagida-Asanuma E, Faul C, Tomino Y, Kim K, Mundel P. Synaptopodin orchestrates actin organization and cell motility via

regulation of RhoA signalling. Nat Cell Biol 2006; 8: 485-491.

40. Meyer-Schwesinger C, Dehde S, Sachs M, Mathey S, Arefi K, Gatzemeier S, Balabanov S, Becker JU, Thaiss F, Meyer TN. Rho-kinase inhibition prevents proteinuria in immune-complex-mediated antipodocyte nephritis. Am J Physiol Renal Physiol 2012; 303: F1015-1025.

41. Kanda T, Wakino S, Homma K, Yoshioka K, Tatematsu S, Hasegawa K, Takamatsu I, Sugano N, Hayashi K, Saruta T. Rho-kinase as a molecular target for insulin resistance and hypertension. FASEB J 2006; 20: 169-171.

42. Hiroki J, Shimokawa H, Higashi M, Morikawa K, Kandabashi T, Kawamura N, Kubota T, Ichiki T, Amano M, Kaibuchi K, Takeshita A. Inflammatory stimuli upregulate Rho-kinase in human coronary vascular smooth muscle cells. J Mol Cell Cardiol 2004; 37: 537-546.

1 Tables

2 **Table 1.** Summary of immunostaining conditions

Immunohistochemistry	Nephrin	Podocin	Synaptopodin	CD3	B220
First antibody	Rabbit polyclonal antibodies (1:500; IBL, Gunma, Japan)	Rabbit polyclonal antibodies (1:800; IBL)	Mouse monoclonal antibodies (1:50; Fitzgerald, MA, USA)	Rabbit polyclonal antibodies (1:150; Nichirei, Tokyo, Japan)	Rat monoclonal antibodies (1:1000; Cedarlane, Ontario, Canada)
Second antibody	Biotinylated goat anti-rabbit IgG antibodies (SABPO kit, Nichirei)	Biotinylated goat anti-rabbit IgG antibodies (SABPO kit, Nichirei)	Simple Stain Mouse MAX-PO(M) (mouse stain kit, Nichirei)	Biotinylated goat anti-rabbit IgG antibodies (SABPO kit, Nichirei)	Biotinylated goat anti-rat IgG antibodies (Caltag Medsystems, Buckingham, UK)

Immunofluorescence	Nephrin	Podocin	Synaptopodin	CD3	B220
First antibody	Same as in immunohistochemistry	Same as in immunohistochemistry	Same as in immunohistochemistry	/	/
Second antibody	Alexa Fluor 546-labeled donkey anti-rabbit IgG antibodies (1:500, Life Technologies)	Alexa Fluor 546-labeled donkey anti-rabbit IgG antibodies (1:500, Life Technologies)	Alexa Fluor 488-labeled donkey anti-mouse IgG antibodies (1:500, Life Technologies)	/	/

3

4 **Table. 2.** Summary of specific gene primers for real-time polymerase chain

5 reaction

Genes (accession no.)	Primer sequence (5′-3′) F: forward, R: reverse	Product size (bp)	Specific function in podocyte
Nphs1 (NM_019459)	F: ACCTGTATGACGAGGTGGAGAG R: TCGTGAAGAGTCTCACACCAG	218	SD protein
Nphs2 (NM_130456)	F: AAGGTTGATCTCCGTCTCCAG R: TTCCATGCGGTAGTAGCAGAC	105	SD protein

Synpo (NM_177340.2)	F: CATCGGACCTTCTTCCTGTG R: TCGGAGTCTGTGGGTGAG	90	SD protein
Actn4 (NM_021895)	F: TCCAGGACATCTCTGTGGAAG R: CATTGTTTAGGTTGGTGACTGG	216	Cytoskeletal protein
Cd2ap (NM_009847)	F: CAAGATGCCTGGAAGACGA R: GCACTTGAAGGTGTTGAAAGAG	177	Cytoskeletal protein
Myh9 (NM_022410)	F: AAGGACCAGGCTGACAAGG R: GTCACGACAAATGGCAGGTC	209	Cytoskeletal protein
Podxl (NM_013723)	F: TCCTAAGGCCGTGTATGAGC R: GATGCCATGCAGACGATG	153	Podocyte glycocalyx

Table 3. Clinical parameters of membranous proliferative glomerulonephritis model and control mice

		dsDNA (μg/mL)	sBUN (mg/dL)	sCre (mg/dL)	uACR (μg/mg)
BXSB/MpJ-*Yaa*$^+$	4 months	72.35 ± 4.45	29.80 ± 3.50	0.56 ± 0.17	96.02 ± 54.43
BXSB/MpJ-*Yaa*	4 months	883.07* ± 85.11	38.93 ± 9.92	1.30 ± 1.03	835.20* ± 592.33
C57BL/6	9 months	61.57 ± 19.08	22.88 ± 1.42	0.12 ± 0.01	2.92 ± 0.40
B6.MRL-(*D1Mit202-D1Mit403*)	9 months	85.01* ± 35.86	24.92 ± 5.42	0.21 ± 0.05	29.02* ± 21.57
	15 months	407.55* ± 166.38	30.24 ± 4.63	0.68 ± 0.56	378.61* ± 278.87

Values are mean ± S.E. dsDNA, double-strand DNA; sBUN, serum blood urea nitrogen; sCre, serum creatinine; uACR, urinary albumin-to-creatinine ratio. *Significantly different from each control (Mann–Whitney U test, $P < 0.05$); n $\geqq$ 5.

Table 4. Quantitative evaluations of glomerular damage

	glomerulus damage score	cell number in 1 glomerulus	thickness of glomerular basement membrane (μm)
BXSB/MpJ-*Yaa*$^+$ 4 month	34.01 ± 10.45	35.12 ± 2.33	1.98 ± 0.11
BXSB/MpJ-*Yaa* 4 month	180.68 ± 60.77 *	67.09 ± 9.96 *	4.01 ± 1.69 *
C57BL/6 9month	78.11 ± 21.26	41.12 ± 4.27	2.31 ± 0.08
B6.MRL-(*D1Mit202-D1Mit403*) 15 month	195.96 ± 42.53 *	55.96 ± 3.55 *	5.96 ± 0.98 *

Values are mean ± S.E. *Significantly different from each control (Mann-Whitney *U* test, $P < 0.05$); n ≧ 5.

Table 5. Relation between histological parameters and expression of podocyte functional proteins

	BXSB/MpJ-*Yaa*			B6.MRL-(*D1Mit202-D1Mit403*)		
Parameter/protein	Nephrin	Podocin	Synaptopodin	Nephrin	Podocin	Synaptopodin
CD3-positive cell number	-0.700	-0.600	-0.700	-0.493	0.309	-0.319
B220-positive cell number	-0.308	-0.564	-0.564	-0.030	0.277	-0.577

Values are the Spearman's rank correlation coefficients. n ≧ 5.

Table 6. Relation between clinical parameters and podocyte functional mRNA expression

	BXSB/MpJ-*Yaa*							B6.MRLc1(68-81)						
	SD protein			Cytoskeletal protein			Podocyte glycocalyx	SD protein			Cytoskeletal protein			Podocyte glycocalyx
Parameter /mRNA	*Nphs1*	*Nphs2*	*Synpo*	*Actn4*	*Cd2ap*	*Myh9*	*Podxl*	*Nphs1*	*Nphs2*	*Synpo*	*Actn4*	*Cd2ap*	*Myh9*	*Podxl*
sADA	-0.569*	-0.464	-0.420	-0.662**	-0.310	-0.279	-0.437	-0.557*	-0.121	-0.439	-0.421	-0.275	-0.379	-0.578*
BUN	-0.245	-0.159	-0.203	-0.286	-0.144	-0.256	-0.167	-0.066	-0.170	-0.379	-0.159	-0.352	-0.385	-0.324
sCre	-0.295	-0.110	-0.128	-0.195	-0.121	-0.136	-0.191	0.278	0.109	-0.020	0.154	-0.022	-0.199	-0.003
uACR	-0.624**	-0.512*	-0.747**	-0.865**	-0.624*	-0.574*	-0.621**	-0.505*	-0.245	-0.577**	-0.469*	-0.552**	-0.466*	-0.49*

Values are the Spearman's rank correlation coefficients. SD, slit diaphragm; sBUN, serum blood urea nitrogen; sCre, serum creatinine; uACR, urinary albumin-to-creatinine ratio. * and **, significantly correlated (Spearman's rank-correlation test, $*P < 0.05$. $**P < 0.01$); n $\geqq$ 5.

Figure legends

Figure 1. Histopathology and immune cell infiltration in membranous proliferative glomerulonephritis.

(a–d) Histopathology of renal cortices. BXSB/MpJ-*Yaa*$^{+}$ (BXSB, 4 months; a), BXSB/MpJ-*Yaa* (BXSB-*Yaa*, 4 months; b), C57BL/6 (B6, 9 months; c), and B6.MRL-(*D1Mit202-D1Mit403*) (B6.MRL, 15 months; d). In the glomerulus, mesangial matrix expansion, mesangial cell proliferation, and periglomerular cell infiltration are observed in the BXSB-*Yaa* and B6.MRL mice models. Periodic acid Schiff (PAS) staining. Bars = 50 μm. (e–l) Immunohistochemistry of CD3 (e–h) and B220 (i–l). BXSB (e and i), BXSB-*Yaa* (f and j), B6 (g and k), and B6.MRL (h and k). Bars = 50 μm. CD3-positive cells are observed in the glomerulus and renal interstitium of BXSB-*Yaa* and B6.MRL (arrows). B220-positive cells are observed in the glomerulus of BXSB and BXSB-*Yaa* (arrowheads), but not in B6 and B6.MRL. (m) Numbers of CD3-positive and B220-positive cells in the glomerulus. BXSB and BXSB/MpJ-*Yaa*: 4 months. B6: 9 months. B6.MRL: 15 months. Values are mean ± S.E. *, significantly different (Mann–Whitney *U* test, $P < 0.05$); n = 5.

Figure 2. Ultrastructural changes of the glomerulus in membranous proliferative glomerulonephritis.

(a–j) Ultrastructure of the glomerulus under a transmission electron microscope. BXSB/MpJ-*Yaa*$^{+}$ (BXSB, 4 months; a and f), BXSB/MpJ-*Yaa* (BXSB-*Yaa*, 4 months; b and g), C57BL/6 (B6, 9 months; c and h), B6.MRL-(*D1Mit202-D1Mit403*) (B6.MRL, 9 months; d and i), and B6.MRL (15months; e and j). Compared with the podocytes (Pod) of BXSB and B6, showing clear cytotrabecula (Cyto, which is also known as primary process) and cytopodium (foot process, Fp, which is also known as secondary process) (a, c, f, and h), the Fps of BXSB-Yaa and B6.MRL show irregular arrangements with hypertrophy and partial fusions (b, d, e, g, i, and j). The glomerular basement membrane (GBM) is thickened and wrinkled in BXSB-*Yaa* and B6.MRL (b and e, arrows), and high electron-dense deposits are observed in the double-countered GBM of the subendothelial regions (b and e, asterisks). The slit diaphragm (SD) is a clear linear pattern between the Fps of BXSB and B6 (f and h, arrowheads). In both BXSB-*Yaa* and B6.MRL, the Fp is effaced, and the SD as well as the 3-layer structure of the

GBM are unclear (g, i, and j). Ery, erythrocyte. Bars = 1 μm (a–e) and 100 nm (f–j). (k–t) Ultrastructure of the glomerulus under a scanning electron microscope. BXSB (4 months; k and p), BXSB-*Yaa* (4 months; l and q), B6 (9 months; m and r), B6.MRL (9 months; n and s) and B6.MRL (15 months; o and t). The width of Cyto increase in BXSB-*Yaa* and B6.MRL (l, n, and o) compared with the controls (k and m) and the Fps are unclear in the former Pod. The engagements of each Fp are irregular, and microvillus-like processes (villi) are observed on the surface of Pod in BXSB-*Yaa* and B6.MRL. Bars = 2 μm.

Figure 3. Localizations of podocyte functional markers in membranous proliferative glomerulonephritis.

(a–l) Immunofluorescence of nephrin (a–d), podocin (e–h), and synaptopodin (i–l). BXSB/MpJ-*Yaa*$^{+}$ (BXSB, 4 months; a, e, and i), BXSB/MpJ-*Yaa* (BXSB-*Yaa*, 4 months; b, f, and j), C57BL/6 (B6, 9 months; c, g, and k), and B6.MRL-(*D1Mit202-D1Mit403*) (B6.MRL, 15 months; d, h, and l). The positive reactions for nephrin, podocin, and synaptopodin tended to be faint, partially showed granular patterns, and localized to the glomerular edge

rather than the center in BXSB-*Yaa* and B6.MRL glomeruli. Bars = 50 μm. (m) Comparison of SD protein–positive area ratio. The relative immune-positive areas of nephrin, podocin, and synaptopodin in the glomerulus. BXSB and BXSB/MpJ-*Yaa*: 4 months. B6: 9 months. B6.MRL: 15 months. Values are mean ± S.E. *, significantly different from each control mice (Mann–Whitney *U* test, $P < 0.05$); n = 5.

Figure 4. mRNA expression levels of podocyte functional markers in membranous proliferative glomerulonephritis.

The relative mRNA expression of podocyte functional markers was analyzed by quantitative real-time PCR, using isolated glomerulus samples. BXSB/MpJ-*Yaa*$^{+}$ (BXSB, 4 months), BXSB/MpJ-*Yaa* (BXSB-*Yaa*, 4 months), C57BL/6 (B6, 9 months), and B6.MRL-(*D1Mit202-D1Mit403*) (B6.MRL, 9 and 15 months). Each podocyte functional marker was normalized to *Actb*. Values are mean ± S.E. *, significantly different from each control mice (Mann–Whitney *U* test, $P < 0.05$); n $\geqq$ 4.

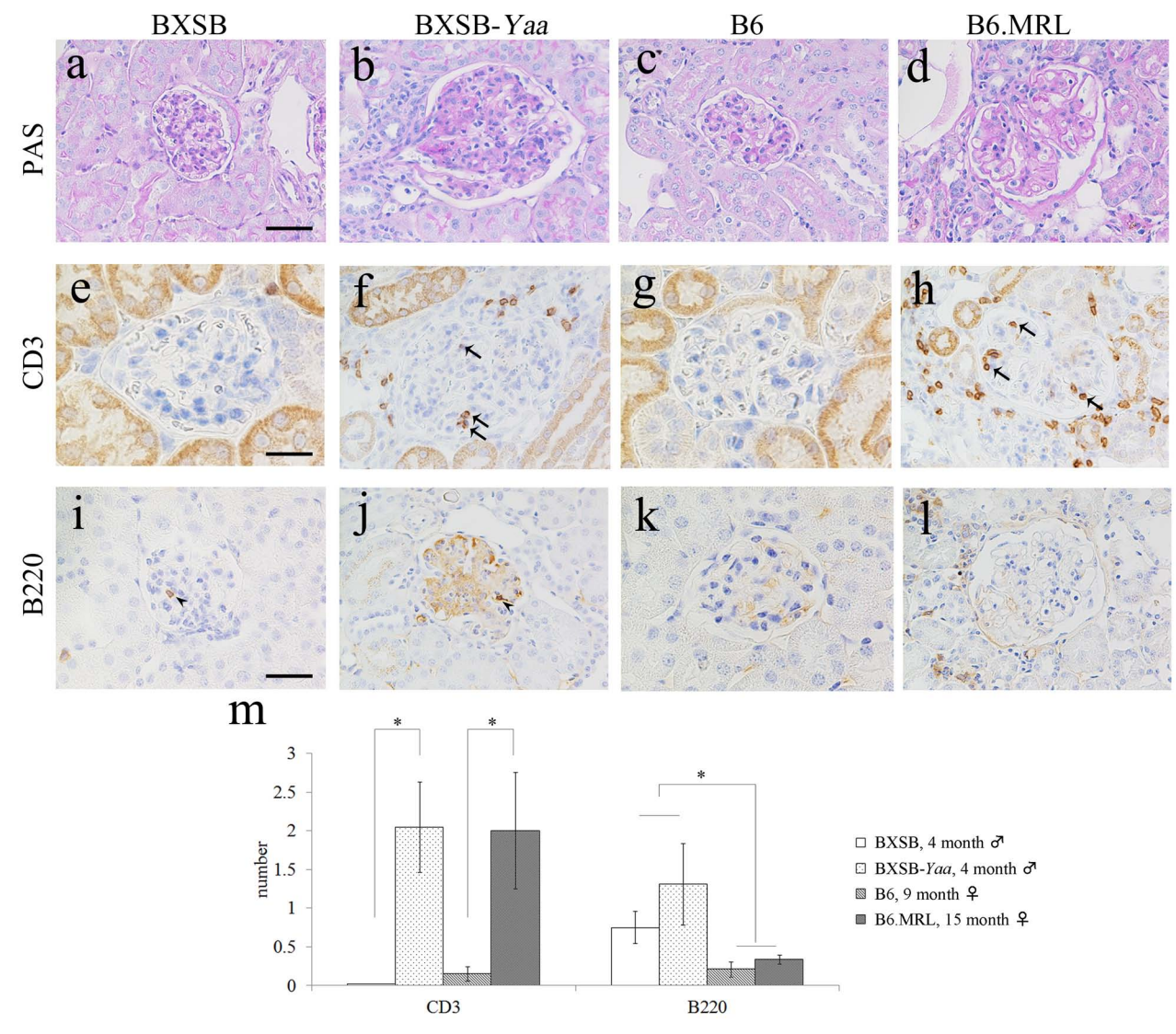
BXSB
BXSB-Yaa
B6
B6.MRL
PAS
CD3
B220
a
b
c
d
e
f
g
h
i
j
k
l
m
number
3
2.5
2
1.5
1
0.5
0
*
*
*
CD3
B220
BXSB, 4 month ♂
BXSB-Yaa, 4 month ♂
B6, 9 month ♀
B6.MRL, 15 month ♀

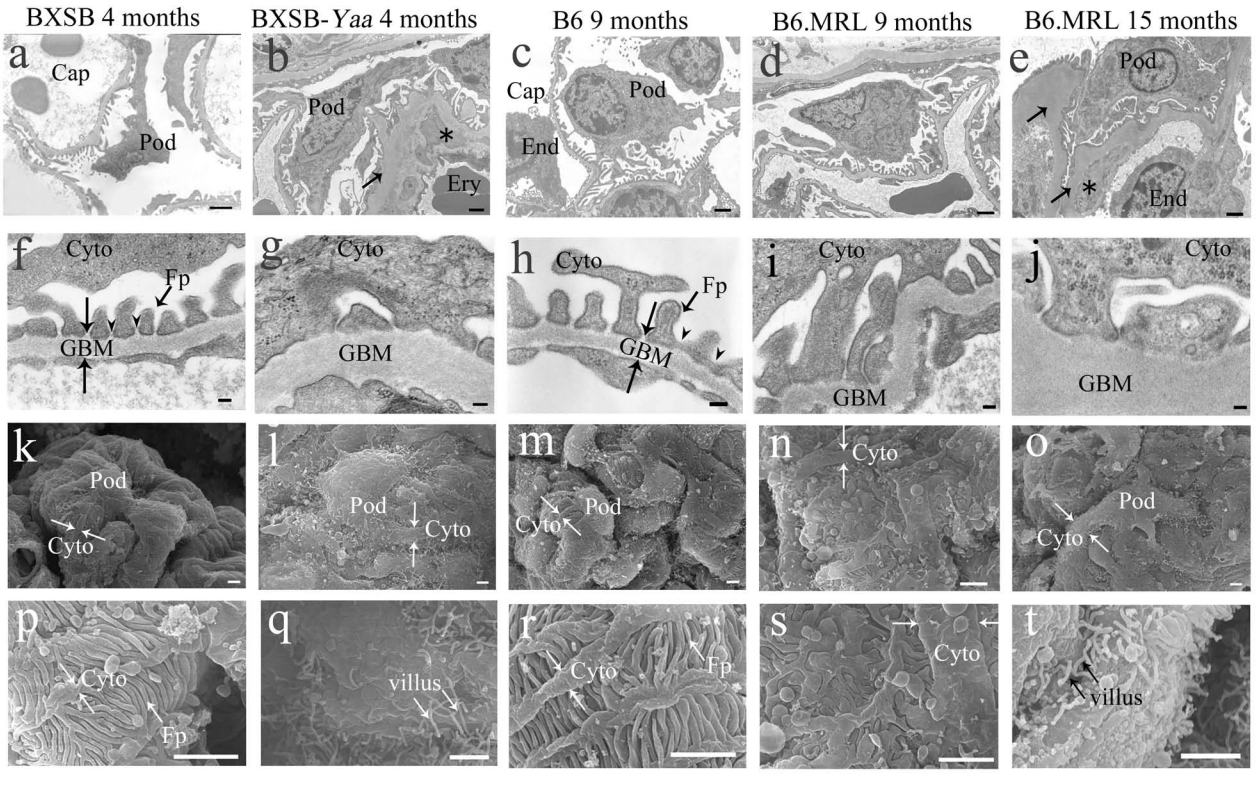
BXSB 4 months
BXSB-Yaa 4 months
B6 9 months
B6.MRL 9 months
B6.MRL 15 months
a
Cap
Pod
b
Pod
*
Ery
c
Cap
Pod
End
d
e
Pod
*
End
f
Cyto
Fp
GBM
g
Cyto
GBM
h
Cyto
Fp
GBM
i
Cyto
GBM
j
Cyto
GBM
k
Pod
Cyto
l
Pod
Cyto
m
Cyto
Pod
n
Cyto
o
Pod
Cyto
p
Cyto
Fp
q
villus
r
Cyto
Fp
s
Cyto
t
villus

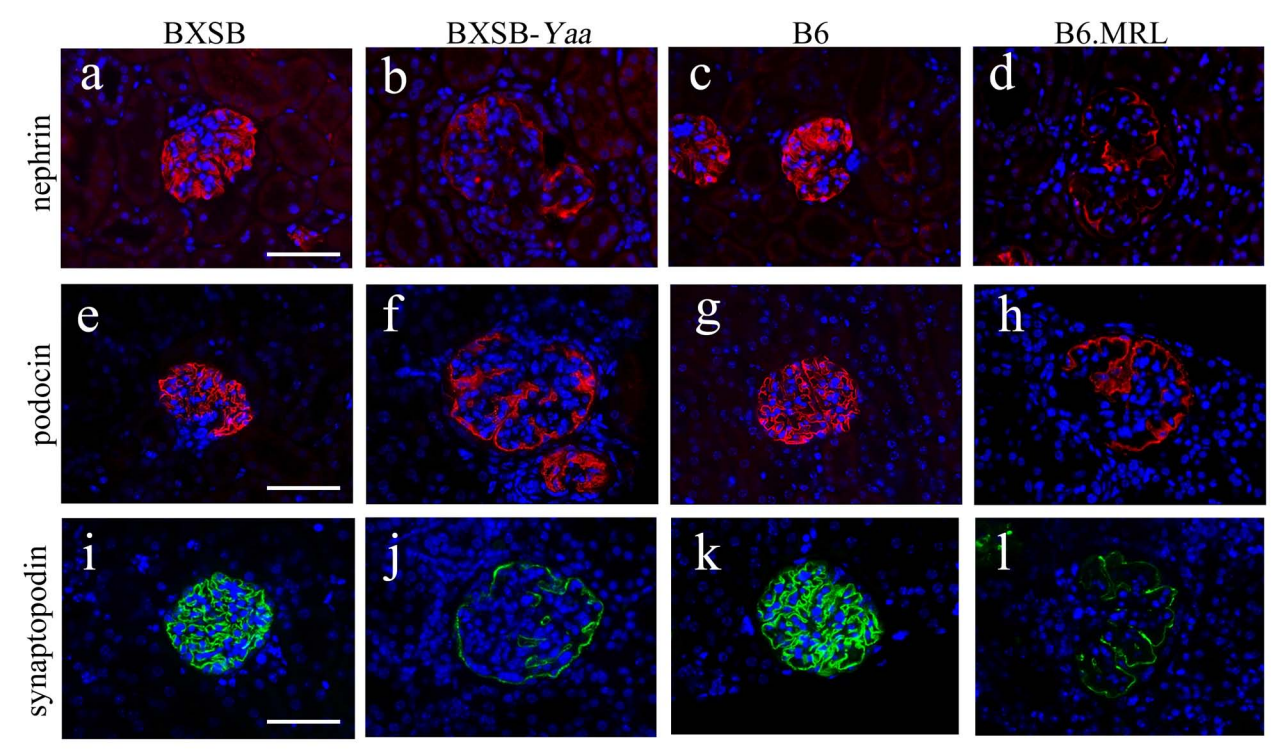
BXSB
BXSB-Yaa
B6
B6.MRL
nephrin
podocin
synaptopodin
a
b
c
d
e
f
g
h
i
j
k
l

m

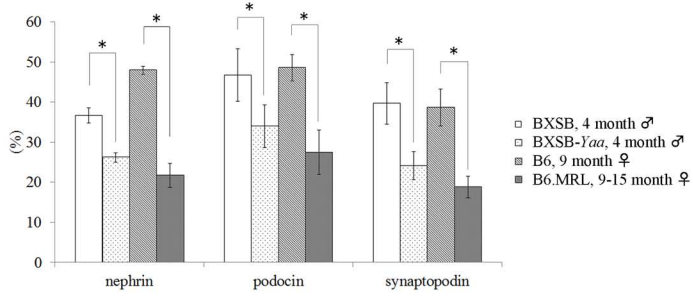
60
50
40
30
20
10
0
(%)
*
nephrin
podocin
synaptopodin
BXSB, 4 month ♂
BXSB-Yaa, 4 month ♂
B6, 9 month ♀
B6.MRL, 9-15 month ♀

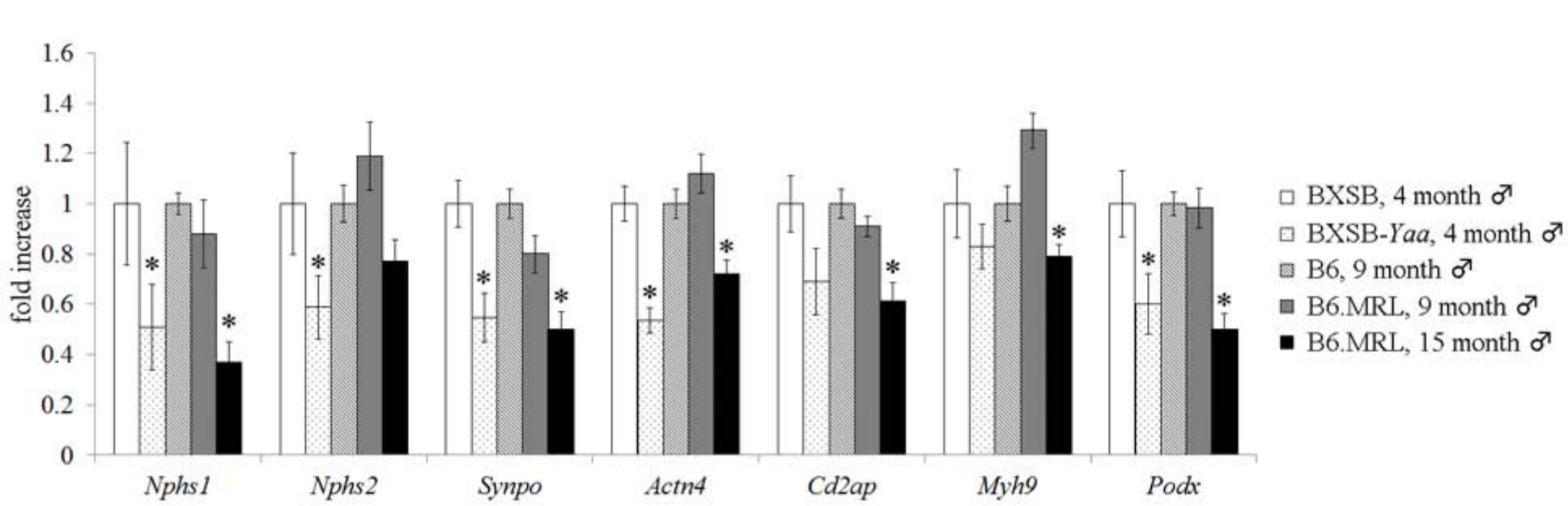
1.6
1.4
1.2
1
0.8
0.6
0.4
0.2
0
fold increase
Nphs1
Nphs2
Synpo
Actn4
Cd2ap
Myh9
Podx
BXSB, 4 month ♂
BXSB-Yaa, 4 month ♂
B6, 9 month ♂
B6.MRL, 9 month ♂
B6.MRL, 15 month ♂

Supplementary material 1

Histological Analysis

Glomerular damage scores were determined according to the following procedures. Briefly, 100 glomeruli per kidney was examined by using PAS-stained sections and scored from 0 to +4 according to the following criteria: 0, no recognizable lesion in glomeruli; +1, a little PAS-positive deposition, mild cell proliferation, mild membranous hypertrophy, and/or partial podocyte adhesion to the parietal layer of the renal corpuscle; +2, segmental or global PAS-positive deposition, cell proliferation, membranous hypertrophy, and/or glomerular hypertrophy; +3, the same as grade 2 with PAS-positive deposition in 50% of regions of glomeruli and/or severe podocyte adhesion to the parietal layer of the renal corpuscle; +4, disappearance of capillary and capsular lumina, global deposition of PAS-positive material, and/or periglomerular infiltration of inflammatory cells and fibrosis, based on the degrees of PAS-positive deposition, cell proliferation, membranous hypertrophy, podocyte adhesion to the parietal layer, disappearance of capillary and capsular lumina, and periglomerular infiltration of inflammatory cells and fibrosis. If, for example, 50 of 100 glomeruli were +1, 25 of 100 glomeruli were +2, 20 of 100 glomeruli were +3, and 5 of 100 glomeruli were +4, the semiquantitative score would be $\{(1 \times 50 / 100) + (2 \times 25 / 100) + (3 \times 5 / 100) + (4 \times 5 / 100)\} \times 100 = 180$.

To assess the glomerular and membranous lesions, cell number in 1 glomerulus and GBM thickness were determined, respectively. The number of cells per glomerulus and thickness of thickest GBM in 1 glomerulus were determined and averaged in at least 10 glomeruli of the PAS-stained samples.

Immunohistochemistry

Immunostaining for nephrin, podocin, synaptopodin, CD3, and B220 was performed according to the following procedure. For antigen retrieval, deparaffinized sections were incubated in citrate buffer (pH 6.0) for 20 min at 105°C for nephrin and podocin (Dako Target Retrieval Solution, pH 9; DAKO, Glostrup, Denmark), for 20 min at 105°C for synaptopodin and CD3, or in 0.1% pepsin/0.2 M HCl for 5 min at 37°C for B220. After cooling, slides were soaked in methanol containing 3% H_2O_2 for 15 min at room temperature. After washing, sections were blocked by 10% normal goat serum for nephrin and podocin, blocking solution A (mouse stain kit; Nichirei, Tokyo, Japan) for synaptopodin, or 0.25% casein/0.01 M PBS for CD3 and B220 for 60 min at room temperature. Then, sections were incubated with rabbit polyclonal antibodies for nephrin (1:500; Immuno-Biological Laboratories, Gunma, Japan), rabbit polyclonal antibodies for podocin (1:800; Immuno-Biological Laboratories), mouse monoclonal antibodies for synaptopodin (1:50; Fitzgerald, MA, USA), rabbit polyclonal antibodies for CD3 (1:150; Nichirei), or rat monoclonal antibodies for B220 (1:1000; Cedarlane, Ontario, Canada) overnight at 4°C. After washing 3 times in phosphate-buffered saline (PBS), sections were incubated with biotin-conjugated goat anti-rabbit IgG antibodies for nephrin, podocin, and CD3 (SABPO kit, Nichirei) or goat anti-rat IgG antibodies for B220 (1:200; Caltag Medsystems, Buckingham, UK) for 30 min at room temperature, washed, and incubated with streptavidin-biotin complex (SABPO kit, Nichirei) for 30 min. For synaptopodin, sections were incubated with blocking solution B (mouse stain kit, Nichirei) for 10 min at room temperature, washed, and incubated with Simple Stain Mouse MAX-PO(M) (mouse stain kit, Nichirei) for 10 min. All sections were then incubated with 3,3′-diaminobenzidine tetrahydrochloride–H_2O_2 solution. Finally, the

sections were counterstained with hematoxylin.

Immunofluorescence

Immunofluorescence for nephrin, podocin, and synaptopodin was performed according to the following procedure. After the deparaffinization, antigen retrieval was performed by same method as in immunohistochemistry. After being washed, sections were blocked by 5% normal donkey serum for 60 min at room temperature. Incubation with primary antibodies was performed by same method as in immunohistochemistry. After washing with PBS, the sections were incubated with Alexa Fluor 546-labeled donkey anti-rabbit IgG antibodies (1:500, Life Technologies) for nephrin and podocin, or Alexa Fluor 488-labeled donkey anti-mouse IgG antibodies (1:500, Life Technologies) for synaptopodin for 30 min at room temperature and washed again. For nuclear staining, sections were incubated with Hoechst 33342 (1:2000; Dojindo, Kumamoto, Japan) for 5 min.